

Northern *JHK* Standard Stars for Array Detectors

L. K. Hunt, F. Mannucci
C. A. I. S. M. I. - C. N. R.

L. Testi¹, S. Migliorini, R. M. Stanga
Dipartimento di Astronomia, Università di Firenze
and

C. Baffa, F. Lisi, L. Vanzi²
Osservatorio Astrofisico di Arcetri

ABSTRACT

We report *J*, *H*, and *K* photometry of 86 stars in 40 fields in the northern hemisphere. The fields are smaller than or comparable to a 4×4 arcmin field-of-view, and are roughly uniformly distributed over the sky, making them suitable for a homogeneous broadband calibration network for near-infrared panoramic detectors. *K* magnitudes range from 8.5 to 14, and *J* – *K* colors from -0.1 to 1.2. The photometry is derived from a total of 3899 reduced images; each star has been measured, on average, 26.0 times per filter on 5.5 nights. Typical errors on the photometry are $\sim 0^m012$.

Subject headings: methods: data analysis — techniques: photometric

arXiv:astro-ph/9803153v2 14 May 1999

¹Current Address: CalTech, Pasadena, CA, USA

²Current Address: CAISMI-CNR, Firenze, Italy

1. Introduction

The widespread availability of near-infrared (NIR) panoramic detectors has rendered possible many scientific programs which were unfeasible with single-element photometers. New and more sophisticated data acquisition and reduction techniques have successfully exploited the capabilities of the new technology while, at the same time, photometric calibration has generally relied on older pre-existing standard networks based on “one-pixel” photometry. Such networks include the SAAO system of Glass (1974), expanded and rationalized by Carter (1990, 1995), comprising probably the most comprehensive and best-observed list available; the MSO system defined by Jones & Hyland (1980, 1982), now more or less supplanted or absorbed into the AAO system (Allen & Cragg 1983); the ESO system (Engels 1981; Bouchet, Schmider, & Manfroid 1991); and the system which appears to the greatest extent to have inherited the original mantle of the photometry of H. L. Johnson in the 1960s, the CIT (Caltech/Cerro-Tololo) system of Frogel et al. (1978) updated by Elias et al. (1982). This last forms the basis of the unpublished, but widely used, hybrid standard star set maintained at the 3.8 m UK Infrared Telescope (UKIRT).

All these comprise relatively bright stars suitable for photometry at small- and medium-sized telescopes with instruments which do not have the limited well capacities of array elements. However, when observed with array detectors even on moderate-sized telescopes, stars with $K \lesssim 7.5$ produce saturated pixels unless defocused or observed in non-standard modes with extremely short on-chip integration times, neither of which stratagem is conducive to precise and homogeneous calibration.

The “UKIRT Faint Standards” (Casali & Hawarden 1992) upon which the calibration of this work is based comprise a new set of much fainter stars chosen and observed at UKIRT to facilitate observations with panoramic detectors with limited dynamic range. However, they are relatively few in number and isolated, occur mostly around the celestial equator, and many of the stars are too faint to be useful for small- or medium-sized telescopes. Only preliminary results are currently available for the UKIRT Faint Standards, although this situation is actively being remedied by the expansion and reobservation of the list at UKIRT.

We present here a set of J , H , and K photometric measurements, obtained with the Arcetri NICMOS3 camera, ARNICA. The photometry comprises 86 stars in 40 fields observable from the northern hemisphere. The selection of the standard fields is described in Section 2, followed by

a discussion of observing and data reduction techniques in Section 3. Section 4 presents the photometry and a comparison with other photometric systems.

2. The Sample Fields

The sample was designed around the capabilities of the large-format NICMOS and InSb arrays mounted in cameras at small- to medium-sized telescopes. In particular, stars with relatively faint K magnitudes were required ($8.5 \lesssim K \lesssim 14.0$), with as wide a color range as possible ($-0.2 \lesssim J-K \lesssim 1.0$). Moreover, the calibrated stars should be situated in relatively uncrowded fields so as to avoid confusion and facilitate field identification. At the same time, more than one calibrated star should be available in a 2×2 arcmin field-of-view (FOV). Finally, the range in apparent position was chosen to provide good sky coverage for northern hemisphere sites with latitudes between 35 and 45° .

To facilitate initial calibration and minimize the effects of color terms, we selected a set of 15 SAO stars with spectral type A0 and V magnitudes of roughly 9. These SAO stars are distributed uniformly in R.A and about a declination of 40° . The similarity of A-star NIR and visual magnitudes makes possible an instantaneous initial rough calibration and provides easy consistency checks. A stars have the further advantage that they tend not to be variable, and, notwithstanding their relatively faint infrared magnitudes, are easily visible at the telescope.

Because we wanted to exploit the two-dimensional capability of panoramic detectors, we added to the list fields taken from the CCD standard stars given in Christian et al. (1985). These fields comprise a large range in optical magnitude, are minimally crowded, and are observable with a 2×2 arcmin FOV. All of the fields are in the vicinity of star clusters.

Stars selected from the UKIRT faint standard system (Casali & Hawarden 1992) were used as primary calibration sources. We extracted from the UKIRT list of faint standards those stars with declinations $\geq 0^\circ$ and with K magnitudes $\gtrsim 8.5$; $J-K$ colors for this subset range from -0.2 to 0.6 . The UKIRT list comprises optical standards from “selected areas” (Landolt 1983), HST calibration objects (Turnshek et al. 1990), and stars in M67 (Eggen & Sandage 1964) and in the globular clusters M3 (NGC 5272) and M13 (NGC 6205). Stars surrounding the nominal calibration stars in the UKIRT fields were used as program objects, and processed in the same way as the A-star and CCD fields mentioned above.

Our goal was to calibrate as many stars as possible within the central FOV of the camera ob-

servations. Many of the central stars proved to be relatively isolated, so that the mean number of stars per field is $\gtrsim 2$. The list of fields with coordinates of the individual stars for which we obtained photometry is given in Table 1. The coordinates were determined from the Digitized Sky Survey³. *K*-band finding charts for the 40 fields are illustrated in Fig. 1.

Fig. 1.— *K*-band finding charts. The field-of-view (FOV) is roughly 4×4 arcmin, and a 1 arcmin segment is shown in the upper-left panel in each page of the figure; AS 39 has a smaller FOV, but the same scale, as suggested by the white border. The finding charts are oriented with N up, and E to the left. Central stars are labelled with a “0”, and field stars with arbitrary sequential numbers, as also given in Table 1.

3. Observations and Data Treatment

J ($1.2\mu\text{m}$), *H* ($1.6\mu\text{m}$), and *K* ($2.2\mu\text{m}$) broad-band images of the standard star fields were acquired with the Arcetri NIR camera, ARNICA, mounted at three telescopes: 1) the 1.5-m f/20 Gornergrat Infrared Telescope⁴ (TIRGO); 2) the 2.56-m f/11 Nordic Optical Telescope⁵ (NOT); 3) the 1.8-m f/9.5 Vatican Advanced Technology Telescope⁶ (VATT). Data were obtained on 31 photometric nights in six runs from December, 1992, to April, 1997; only 10 of these nights were dedicated exclusively to this project.

The camera, ARNICA, relies on a NICMOS3 256×256 1–2.5 μm HgCdTe scientific grade array, and provides a 4×4 arcmin FOV with 1 arcsec pixels at the TIRGO, and 2×2 arcmin with 0.5 arcsec pixels at the VATT and the NOT. Details of the camera design and implementation are given in Lisi et al. (1993, 1996), and of the characterization of the detector and camera performance in Hunt et al. (1994a, 1996).

³The images on these disks are based on photographic data obtained using the Oschin Schmidt Telescope on Palomar Mountain. The Palomar Observatory Sky Survey was funded by the National Geographic Society. The Oschin Schmidt Telescope is operated by the California Institute of Technology and Palomar Observatory. The plates were processed into the present compressed digital form with their permission. The *Digitized Sky Survey* was produced at the Space Telescope Science Institute under U. S. Government grant NAG W-2166.

⁴The TIRGO (Gornergrat, Switzerland) is operated by CAISMI-CNR, Arcetri, Firenze.

⁵The NOT is operated on the island of La Palma jointly by Denmark, Finland, Norway, Sweden, in the Spanish Observatorio del Roque de los Muchachos of the Instituto de Astrofísica de Canarias.

⁶The VATT (Mount Graham, Arizona) is composed of the Alice P. Lennon Telescope and the Thomas J. Bannan Astrophysics Facility, both operated by the University of Arizona (Steward Observatory) and the Vatican Observatory Research Group.

For each observation with each filter, the center of the field was placed in five different positions on the array: the first near the center, and the remaining four in the center of each of the four quadrants. For *J* and *H*, sky frames were used as the flat field correction. To account for telescope emissivity at $2\mu\text{m}$, *K*-band observations were instead reduced using differential flat fields, obtained independently. Tests showed that these procedures minimize the residual (after flat-field correction) spatial variation in the photometry (see Appendix). All the data reduction was carried out with the ARNICA data reduction package (Hunt et al. 1994c) in the IRAF⁷ environment.

The images acquired in the first two (commissioning) runs – about one-third of the database – showed a residual spatial variation in the photometry that was subsequently rectified by a modification in the camera optics. To correct for this effect in those runs, an empirical second-order flat-field correction was applied to each image as described in Hunt et al. (1994b, 1996). We have checked that this procedure produces no systematic trends relative to the later data.

3.1. Photometry

Virtual aperture photometry was performed for each of the different positions separately. The technique of moving the telescope to place the star in different positions on the array implies that five measurements are available for the central stars, but that field stars may have fewer measurements because they may fall outside the array. Note that we used relatively large apertures in order to encompass possible faint stars within 10 arcsec of the program stars. Images with discrepant values for the photometry were checked to evaluate effects of any bad pixels, and these were either corrected, when possible, or eliminated from further consideration.

Observations of the UKIRT faint standards throughout the night were used to determine the nightly “zero point” (zp) for each band. From five to eight stars from the UKIRT Faint Standard list were observed each night together with the program stars. Most of the program star observations were obtained at 1.6 airmasses or less, and every attempt was made to observe the calibrating stars over the same range in airmass as the program stars. Atmospheric extinction was corrected for by fitting simultaneously, for each band for each run, an extinction coefficient common to all nights and a zp that varied from night to night. Typi-

⁷IRAF is the Image Analysis and Reduction Facility made available to the astronomical community by the National Optical Astronomy Observatories, which are operated by AURA, Inc., under contract with the U.S. National Science Foundation.

cal extinction coefficients are ~ -0.06 , 0.0 , and -0.04 mag/airmass at J , H , and K , respectively.

In total, we calibrated 86 stars in 40 fields in J , H , and K filters; the photometry is reported in Table 1. The final values for the photometry of the program stars were determined by combining, in a weighted average, all the measurements, corrected for extinction, from the different nights of observation. The errors given in Table 1 are the errors on the mean. The exact prescription for these calculations is given in the Appendix. For a few stars (e.g., AS16-1, AS39-1), the errors in one band are much smaller than the errors in the remaining bands; these small errors probably result from an observed scatter which is fortuitously small, and thus the larger errors in the remaining bands may be a more realistic estimate of the quality. We note that the colors in the table are merely the differences of the mean magnitudes, as we determined the photometry in each filter band separately, instead of giving precedence to one band and determining mean colors.

4. Results and Discussion

The final database contains 6551 photometric measurements from 3899 reduced images. On average, stars have been observed on 26.0 times per filter on 5.5 different nights, but a few have been observed on only three nights (see Table 1), and these should probably be used with more discretion than the rest. The median (mean) error in the photometry in Table 1 is $0^{\text{m}}012$ ($0^{\text{m}}013$), $0^{\text{m}}011$ ($0^{\text{m}}012$), and $0^{\text{m}}011$ ($0^{\text{m}}012$), in J , H , and K , respectively. No photometric value in the Table has a formal error $> 0^{\text{m}}028$, and standard deviations of the ensemble of values used to calculate the photometry are always $\leq 0^{\text{m}}05$. Figure 2 illustrates this quality assessment. For a given star, the measurements taken in the same night are not considered as statistically independent values, since they were calibrated with the same zp and, in a given five-position set, reduced with inter-dependent sky frames.

We note that the filling factor of the NICMOS3 array is roughly 95%. The projected pixel dimension at all telescopes was typically half the typical seeing width, so that the mean photometric error due to an incompletely filled array element is $\lesssim 0.1\%$ (McCaughrean 1988), and should be negligible relative to the other sources of scatter.

The $J-H$ and $H-K$ colors for the stars listed in Table 1 are shown in Fig. 3. It can be seen from the figure that the stars in our data set span a wide range in spectral type, notwithstanding the initial selection of a preponderance of A stars. The $J-K$ color ranges from -0.2 to $\gtrsim 1.2$, making possible accurate evaluations of color transformations between this photometry and other work.

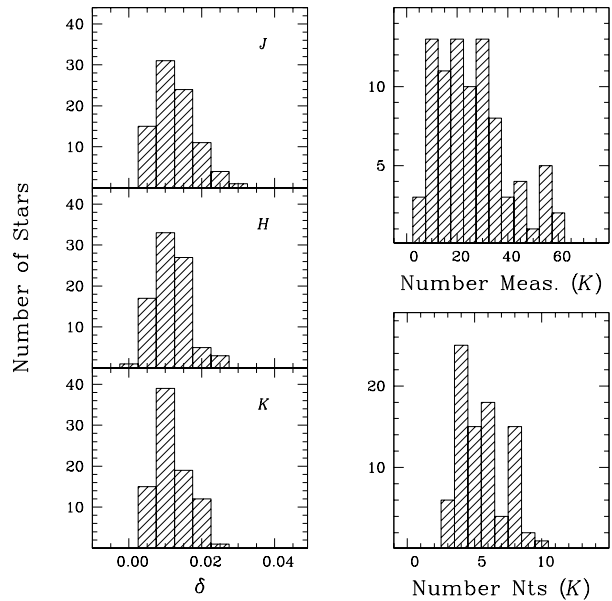


Fig. 2.— Histograms of J , H , and K errors for the photometry reported in Table 1, number of measurements (frames), and number of different nights. Numbers of measurements and nights are shown for the K band only. The calculation of the errors of the mean δ shown in the left panels is described in the Appendix.

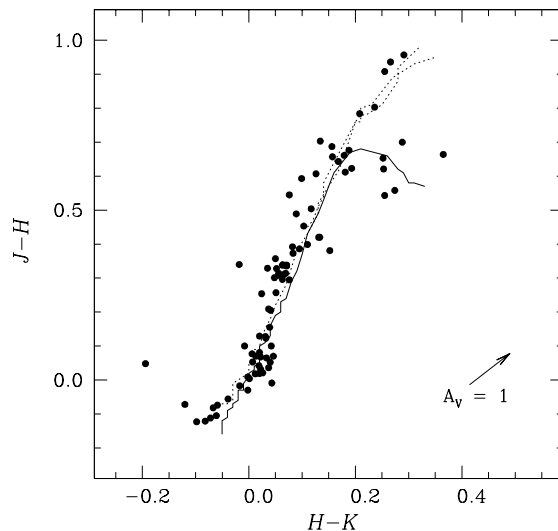


Fig. 3.— $J-H$ vs. $H-K$ colors for the stars listed in Table 1. The solid line traces the main sequence (Koornneef 1983), and the dotted lines the giants and supergiants. A unit V -magnitude extinction is shown by the arrow in the lower right-hand corner. The isolated point with $J-H \sim 0$ and $H-K \sim -0.2$ is FS 14.

We have checked for correlations of reported errors with $J - K$ color or magnitude, and find no trend with color. The only (very weak) correlation is with K -band errors and K magnitude, such that errors are larger for fainter stars. This is not unexpected behavior, since the faintest stars suffer the most from the large K -band background (typically 12–12.5 mag arcsec⁻²), and the consequent uncertainty in its subtraction. Although our data are well-suited to searches for variability, given the long month/years timescales spanned by our observations, we found no convincing evidence for variation. Nevertheless, a more definitive statement awaits long-term monitoring, in particular, of the reddest stars.

4.1. Comparison with UKIRT Photometry and Transformation Equations

Of the 86 stars in Table 1, 22 are UKIRT Faint Standards (denoted as “FS” in the Table), and were used to calibrate the photometry. The residuals for these stars were defined, similarly to the magnitudes of the program stars, as the mean difference, over all the nights of observation, between the nightly zp and the zp of the star itself. Their magnitudes, in the system described here, were determined from the sum of the nominal UKIRT magnitudes and the mean residuals. The mean residuals of the UKIRT faint standards (omitting FS 14, see below) are 0.001, -0.0004, and -0.004 in J , H , and K , respectively, and with RMS differences of 0.012, 0.013, and 0.019. We therefore measure no significant offset between the ARNICA photometry reported here, and the UKIRT system from which it was derived.

Of the 22 UKIRT Faint Standards, three stars, FS 14, FS 21, and FS 33, have significant non-zero residuals relative to the published UKIRT photometry (Casali & Hawarden 1992). The star with the largest residual ($\Delta H = -0^m061$ with S/N = 2.5), FS 14, is also the faintest star used as a calibrator. Hence, it was subsequently treated as a program object and removed from the list of calibrators; for all of the nights in which it was observed, the nightly calibration was redone, and the photometry recalibrated.

We have attempted to derive a color transformation equation between the photometry published here and the original UKIRT system. (A transformation equation between UKIRT and CIT has been published in Casali & Hawarden (1992).) The ARNICA J -, H -, and K -band residuals (in the sense ARNICA – UKIRT) for the UKIRT calibrator stars and UKIRT $J - K$ color were fit with weighted regressions. (FS 14 was omitted from this operation.) The only (possibly) significant non-zero slope is for J with $\Delta J = -0.015(J - K)_{UKIRT} + 0.0046$; this regression is shown as

a dashed line in the lower panel of Fig. 4. Although the ARNICA J filter may be slightly redder than the UKIRT one, as suggested by the above equation, the data used to determine the regression are not suited to this kind of analysis. The color excursion of the UKIRT FS’s is limited ($J - K \sim -0.02 - +0.6$), and there is a trend between color and magnitude such that the bluest stars are also the faintest, and thus subject to the largest uncertainty. We caution, therefore, that these values for a J -band color transformation should be considered as very preliminary.

5. Conclusions and Summary

We have presented new NIR photometry for 86 stars in 40 fields. The sky coverage is relatively uniform, and ideal for observatories with $\delta \gtrsim 30^\circ$. On average, stars have been observed on more than five different nights, and typical errors on the photometry are 0^m.012. We find some indication of a color transformation between the ARNICA (NICMOS) photometry reported here and the original UKIRT (InSb) system, but a definitive statement awaits a larger data set designed specifically to determine such a transformation.

The staffs of the TIRGO, the NOT, and the VATT helped make these observations possible. We are grateful to Colin Aspin, Mark Casali, and Tim Hawarden for insightful comments and useful advice; to Prof. Gianni Tofani for his generosity in funding the expenses of publication; and to an anonymous referee for helpful criticism and comments on an earlier version of this paper.

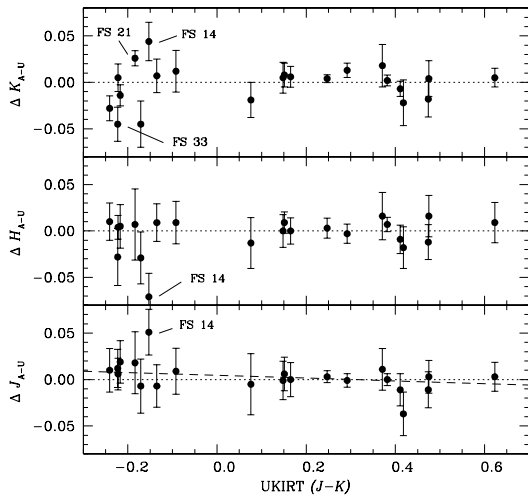


Fig. 4.— J -, H -, and K -band residuals shown as a function of UKIRT $J - K$; the sense is ARNICA (this paper) - UKIRT. Error bars are the quadrature sum of the errors associated with the original UKIRT photometry (Casali & Hawarden 1992), and the errors shown in Table 1. Residuals constant with $J - K$ color are shown by dotted lines, and the lower panel shows the weighted regression (dashed line) of J -band residuals with $J - K$ color. Also indicated are the three stars with significant residuals as described in the text.

A. Calculation of the Means and Errors in Table 1

There are two main sources of error or uncertainty in our data: residual spatial variation in the photometry (that is to say after the flat-field correction), and variation in the atmospheric transparency. In order for our error estimate to be reliable, we must be able to separate these effects, and realistically assess their impact. We note that residual spatial variation is observed only with the optics used at the TIRGO. The largest-amplitude effect was observed in the commissioning runs (1992-93), and was corrected for by an empirically-determined flat field mentioned in the main text, and described in detail in Hunt et al. (1996). The TIRGO optical train was then modified, and typical subsequent runs at TIRGO are characterized by roughly 0.05 mag scatter, a value which comprises both atmospheric and spatial variation. Runs at the VATT and the NOT do not show measurable spatial variation in the photometry.

We describe here how the individual measurements were combined into the final mean magnitudes reported in Table 1. The nightly magnitudes for each star and their associated errors are described first, followed by the description of the final averages. As noted in the main text, in each filter, a single observation consists of at least five frames (“measurements”) with the star placed in different positions on the array. In what follows, σ will be used to denote exclusively the standard deviation of a given ensemble. The *errors* we associate with a given value will be denoted by δ .

First, the variation in the atmospheric transparency σ_t for each night was determined by the global fit, over an entire run, of the extinction coefficients and nightly zero points (zp) at unit air mass. The photometry used for this fit was averaged over position, and thus, as long as this averaging procedure is free of systematics, should be independent of spatial variation. The fit gives nightly zp’s with formal errors, and these last define σ_t .

The residual spatial variation in the photometry was managed by using, when possible, positional zp’s (zp_p) to separately calibrate the program star measurements at each position. Such a procedure does not change the nightly mean, but reduces the impact of any spatial variation in the photometry, which is at least partially compensated by the equivalent spatial variation in the calibrator. If on a given night n we have I_n measurements $f_*(p, n)$ of a given star, then we can de-

fine $m_{p,n} = -2.5 \log f_*(p, n) + zp_{p,n}$, where subscript p indicates the position on the array. The nightly mean magnitude m_n was determined by a simple average over the I_n measurements $m_{p,n}$. Typically, I_n is 5 for central stars, and less for field stars sufficiently distant from the central one.

The variance on the ensemble $m_{p,n}$ due to any residual spatial variation can be written as:

$$\sigma_p^2 = \sigma_{x_p}^2 + \sigma_{zp_p}^2 + 2\sigma_{x_p, zp_p} \quad ,$$

where we have defined $x_{p,n} \equiv -2.5 \log f_*(p, n)$; $\sigma_{x_p}^2$ and $\sigma_{zp_p}^2$ are the spatial variances of the x_p and zp_p , respectively, and σ_{x_p, zp_p} is the covariance of the x_p and zp_p . If the photometry varies spatially, then x_p and zp_p are anti-correlated, and the covariance term *reduces* σ_p accordingly. If the use of positionally-dependent zp’s is not possible (for example in the case of the field stars), then σ_p^2 takes into account the increased scatter introduced by any spatial variation.

The final nightly error δ_n associated with m_n was defined as the quadrature sum of the transparency variation σ_t , the uncertainty on the zp given by σ_t/N_{FS} where N_{FS} is the number of calibrators observed on the n^{th} night, and the residual spatial variation (error on the mean):

$$\delta_n = \sqrt{\sigma_t^2 + \sigma_t^2/N_{FS} + \sigma_p^2/I_n} \quad .$$

The global mean of a given star reported in Table 1 is simply the weighted average $\langle m \rangle$ of m_n over all the nights of observations, where the weights are given by $1/\delta_n^2$. The error δ we associate with the final photometry is the error of the mean, defined relative to the weighted average (as opposed to the simple average which would minimize, by definition, the scatter). We chose δ instead of the error of the weighted mean because the former is proportional to the observed final scatter of the data, while the latter is determined exclusively by our estimate of the nightly errors.

REFERENCES

- Allen, D.A. & Cragg, T.A. 1983, MNRAS, 203, 777
- Bouchet, P., Schmider, F.X., & Manfroid, J. 1991, A&ASS, 91, 409
- Carter, B.S. 1990, MNRAS, 242, 1
- Carter, B.S. & Meadows, V.S. 1995, MNRAS, 276, 734
- Casali, M. M. & T. G. Hawarden 1992, JCMT-UKIRT Newsletter, No. 4, 33
- Christian, C.A., Adams, M., Barnes, J.V., Butcher, H., Hayes, D.S., Mould, J.R., & Siegel, M. 1985, PASP, 97, 363
- Eggen, O. J. & Sandage, A. R. 1964, ApJ, 140, 130
- Elias, J. H., Frogel, J. A., Matthews, K., & Neugebauer, G. 1982, AJ, 87, 1029
- Engels, D., Sherwood, W.A., Wamsteker, W., and Shultz, G.V. 1981, A&ASS, 45, 5
- Frogel, J.A., Persson, S.E., Aaronson, M., & Matthews, K. 1978, ApJ, 220, 75
- Glass, I.S. 1974, MNAS Sth. Afr., 33, 53, 71
- Jones, T.J. & Hyland, A.R. 1980, MNRAS, 192, 359
- Jones, T.J. & Hyland, A.R. 1982, MNRAS, 200, 509
- Hunt, L., Maiolino, R., & Moriondo, G. 1994a, Arcetri Observatory Technical Report N. 2/94
- Hunt, L., Maiolino, R., Moriondo, G. & Testi, L. 1994b, Arcetri Observatory Technical Report N. 3/94
- Hunt, L., Testi, L., Borelli, S., Maiolino, R., & Moriondo, G. 1994c, Arcetri Observatory Technical Report N. 4/94
- Hunt, L.K., Lisi, F., Testi, L., Baffa, C., Borelli, S., Maiolino, R., Moriondo, G., & Stanga, R.M. 1996, A&ASS, 115, 181
- Koornneef, J. 1983, A&A, 128, 84
- Landolt, A.U. 1983, AJ, 88, 439
- Lisi, F., Baffa, C., & Hunt, L. 1993, in SPIE Vol. 1946, Infrared Detectors and Instrumentation, ed. A.M. Fowler, 594
- Lisi, F., Baffa, C., Biliotti, V., Bonaccini, D., Del Vecchio, C., Gennari, S., Hunt, L., Marucci, G., & Stanga, R.M. 1996, PASP, 108, 364
- McCaughrean, M. J. 1988, Ph.D. Thesis, University of Edinburgh
- Turnshek, D.A., Bohlin, R.C., Williamson, R.L. II, Lupie, O.L., & Koornneef, J. 1990, AJ, 99, 1243

TABLE 1
ARNICA STANDARD STAR PHOTOMETRY

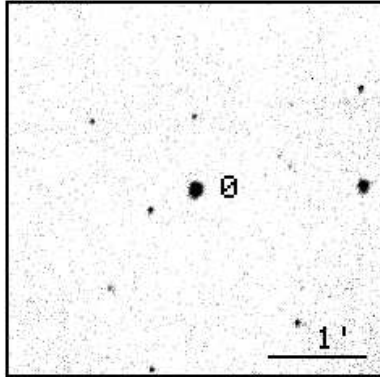
Star Name	Other Designation	Coordinates (2000)		J (δ_J)	H (δ_H)	K (δ_K)	$J - K$	$H - K$	Number Nights ^a
		α	δ						
AS01-0	FS02	00 55 09.9	00 43 13	10.716 (0.005)	10.507 (0.010)	10.470 (0.003)	0.25	0.04	6,6,6
AS02-0	SAO054271	00 55 58.6	39 10 09	8.775 (0.006)	8.771 (0.012)	8.770 (0.009)	0.01	0.00	5,6,6
AS03-0	FS03	01 04 21.6	04 13 39	12.606 (0.011)	12.729 (0.008)	12.827 (0.013)	-0.22	-0.10	6,6,6
AS04-0	FS04	01 54 37.6	00 43 01	10.555 (0.004)	10.301 (0.005)	10.277 (0.006)	0.28	0.02	5,5,5
AS04-1		01 54 43.4	00 43 59	12.371 (0.021)	12.033 (0.020)	11.962 (0.025)	0.41	0.07	4,3,4
AS05-0	FS06	02 30 16.4	05 15 52	13.232 (0.009)	13.314 (0.007)	13.381 (0.010)	-0.15	-0.07	8,7,8
AS05-1		02 30 18.6	05 16 42	14.350 (0.013)	13.663 (0.011)	13.507 (0.009)	0.84	0.16	7,8,8
AS06-0	SAO038218	02 41 03.6	47 41 28	8.713 (0.010)	8.694 (0.014)	8.674 (0.010)	0.04	0.02	8,8,8
AS07-0	FS07	02 57 21.2	00 18 39	11.105 (0.013)	10.977 (0.009)	10.946 (0.010)	0.16	0.03	6,6,7
AS08-0	SAO056596	03 38 08.3	35 10 52	8.744 (0.011)	8.723 (0.014)	8.697 (0.012)	0.05	0.03	5,5,6
AS08-1		03 38 12.0	35 10 11	8.772 (0.011)	7.836 (0.018)	7.570 (0.017)	1.20	0.27	5,5,5
AS08-2		03 38 08.3	35 09 38	9.728 (0.011)	9.121 (0.015)	8.995 (0.016)	0.73	0.13	5,5,6
AS09-0	SAO013053	04 11 05.8	60 10 21	8.432 (0.012)	8.380 (0.014)	8.340 (0.011)	0.09	0.04	6,6,6
AS09-1		04 11 06.2	60 09 39	11.546 (0.015)	10.923 (0.016)	10.730 (0.015)	0.82	0.19	6,6,6
AS10-0	FS11	04 52 58.9	-00 14 41	11.349 (0.011)	11.281 (0.009)	11.259 (0.006)	0.09	0.02	8,8,7
AS11-0	SAO058110	05 29 55.5	39 38 59	9.151 (0.009)	9.181 (0.010)	9.183 (0.011)	-0.03	-0.00	7,8,8
AS11-1		05 30 02.0	39 37 49	11.299 (0.009)	10.342 (0.015)	10.051 (0.008)	1.25	0.29	7,6,6
AS12-0	FS12	05 52 27.4	15 53 23	13.700 (0.018)	13.812 (0.015)	13.884 (0.011)	-0.18	-0.07	5,4,3
AS12-1		05 52 21.5	15 52 44	11.241 (0.007)	10.931 (0.018)	10.866 (0.020)	0.38	0.06	3,4,4
AS13-0	FS13	05 57 07.5	00 01 11	10.517 (0.005)	10.189 (0.005)	10.137 (0.005)	0.38	0.05	9,9,8
AS13-1		05 57 10.4	00 01 38	12.201 (0.019)	11.781 (0.007)	11.648 (0.009)	0.55	0.13	5,5,5
AS13-2		05 57 09.5	00 01 50	12.521 (0.008)	12.101 (0.005)	11.970 (0.006)	0.55	0.13	5,5,5
AS13-3		05 57 08.0	00 00 07	13.345 (0.015)	12.964 (0.017)	12.812 (0.012)	0.53	0.15	5,4,4
AS14-0	SAO013747	06 11 25.4	61 32 15	8.688 (0.013)	8.623 (0.014)	8.590 (0.007)	0.10	0.03	6,6,6
AS14-1		06 11 29.9	61 32 05	9.871 (0.015)	9.801 (0.015)	9.755 (0.011)	0.12	0.05	6,6,6
AS15-0	NGC2264	06 40 34.3	09 19 13	10.874 (0.007)	10.669 (0.010)	10.628 (0.008)	0.25	0.04	8,9,10
AS15-1		06 40 36.2	09 18 60	12.656 (0.011)	11.980 (0.010)	11.792 (0.011)	0.86	0.19	9,9,8
AS15-2		06 40 37.9	09 18 41	13.711 (0.014)	12.927 (0.017)	12.719 (0.012)	0.99	0.21	8,9,8
AS15-3		06 40 37.9	09 18 19	14.320 (0.015)	13.667 (0.017)	13.415 (0.015)	0.91	0.25	8,7,8
AS16-0	FS14	07 24 15.3	-00 32 50	14.159 (0.021)	14.111 (0.011)	14.305 (0.017)	-0.15	-0.19	5,4,4
AS16-1		07 24 14.3	-00 33 05	13.761 (0.020)	13.638 (0.005)	13.606 (0.021)	0.15	0.03	5,4,4
AS16-2		07 24 15.4	-00 32 49	11.411 (0.010)	11.428 (0.017)	11.445 (0.008)	-0.03	-0.02	5,4,4
AS16-3		07 24 17.2	-00 32 27	13.891 (0.012)	13.855 (0.011)	13.818 (0.011)	0.07	0.04	5,4,3
AS16-4		07 24 17.5	-00 33 07	11.402 (0.015)	11.106 (0.019)	11.043 (0.009)	0.36	0.06	4,4,4
AS17-0	NGC2419	07 38 15.5	38 56 16	14.353 (0.012)	14.039 (0.015)	13.983 (0.016)	0.37	0.06	6,5,5
AS17-1		07 38 19.1	38 55 17	12.434 (0.009)	12.077 (0.012)	12.027 (0.017)	0.41	0.05	6,6,6
AS17-2		07 38 16.6	38 57 13	14.745 (0.012)	14.124 (0.012)	13.871 (0.016)	0.87	0.25	5,5,3
AS17-3		07 38 10.7	38 57 11	13.077 (0.007)	12.782 (0.010)	12.706 (0.006)	0.37	0.08	6,6,4
AS17-4		07 38 08.2	38 56 01	14.459 (0.018)	13.795 (0.014)	13.430 (0.018)	1.03	0.37	5,5,5
AS18-0	FS15	08 51 05.8	11 43 47	12.741 (0.008)	12.402 (0.004)	12.338 (0.013)	0.40	0.06	8,8,8
AS18-1		08 51 03.5	11 45 03	10.769 (0.024)	10.614 (0.014)	10.575 (0.014)	0.19	0.04	4,6,6
AS19-0	FS17	08 51 19.7	11 52 11	12.670 (0.014)	12.334 (0.013)	12.263 (0.004)	0.41	0.07	5,5,6
AS19-1		08 51 21.8	11 52 38	10.095 (0.017)	9.794 (0.013)	9.746 (0.010)	0.35	0.05	4,4,5
AS19-2		08 51 20.2	11 52 48	12.745 (0.019)	12.488 (0.024)	12.437 (0.012)	0.31	0.05	4,4,5
AS20-0	SAO042804	09 19 27.5	43 31 46	9.551 (0.012)	9.519 (0.007)	9.497 (0.015)	0.05	0.02	9,9,9

TABLE 1—*Continued*

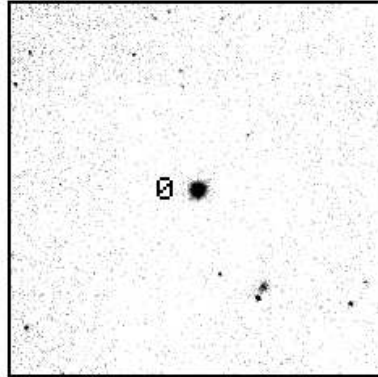
Star Name	Other Designation	Coordinates (2000)		J (δ_J)	H (δ_H)	K (δ_K)	$J - K$	$H - K$	Number Nights ^a
		α	δ						
AS21-0	SAO062058	10 28 42.1	36 46 18	9.061 (0.007)	9.043 (0.015)	9.031 (0.007)	0.03	0.01	6,7,9
AS22-0	FS21	11 37 05.6	29 47 59	12.966 (0.005)	13.038 (0.010)	13.158 (0.007)	-0.19	-0.12	7,7,8
AS23-0	SAO119183	12 02 53.5	04 08 47	8.889 (0.010)	8.847 (0.009)	8.828 (0.010)	0.06	0.02	6,7,6
AS24-0	SAO015832	12 35 15.6	62 56 57	9.398 (0.009)	9.345 (0.009)	9.338 (0.010)	0.06	0.01	5,6,6
AS25-0	FS33	12 57 02.4	22 02 01	14.029 (0.008)	14.134 (0.010)	14.195 (0.009)	-0.17	-0.06	5,4,5
AS26-0	FS23	13 41 43.6	28 29 51	13.000 (0.015)	12.455 (0.012)	12.379 (0.010)	0.62	0.08	7,7,8
AS26-1		13 41 47.2	28 29 49	12.120 (0.016)	11.527 (0.016)	11.428 (0.016)	0.69	0.10	7,8,8
AS27-0	FS24	14 40 07.0	00 01 45	10.910 (0.015)	10.781 (0.007)	10.761 (0.010)	0.15	0.02	5,4,5
AS27-1		14 40 07.3	00 02 23	12.991 (0.015)	12.677 (0.024)	12.608 (0.019)	0.38	0.07	4,3,4
AS28-0	SAO064525	15 09 20.3	39 25 49	8.455 (0.010)	8.378 (0.014)	8.372 (0.008)	0.08	0.01	7,7,8
AS29-0	FS25	15 38 33.3	00 14 19	10.234 (0.005)	9.842 (0.013)	9.760 (0.009)	0.47	0.08	5,5,5
AS29-1		15 38 30.6	00 14 21	13.904 (0.017)	13.566 (0.019)	13.503 (0.020)	0.40	0.06	5,3,4
AS30-0	FS27	16 40 41.6	36 21 13	13.505 (0.004)	13.197 (0.011)	13.141 (0.014)	0.36	0.06	4,4,4
AS30-1		16 40 36.6	36 22 40	12.497 (0.017)	12.157 (0.011)	12.175 (0.021)	0.32	-0.02	3,3,3
AS31-0	FS28	17 44 06.8	-00 24 58	10.744 (0.008)	10.644 (0.005)	10.602 (0.004)	0.14	0.04	6,6,6
AS31-1		17 44 06.2	-00 24 22	12.504 (0.010)	12.131 (0.011)	12.048 (0.007)	0.46	0.08	6,6,6
AS31-2		17 44 04.8	-00 24 11	13.290 (0.009)	12.633 (0.011)	12.476 (0.010)	0.81	0.16	5,5,4
AS32-0	SAO017946	18 36 10.5	65 04 30	8.017 (0.018)	7.917 (0.012)	7.925 (0.014)	0.09	-0.01	4,4,4
AS33-0	FS35	18 27 13.6	04 03 10	12.220 (0.004)	11.834 (0.005)	11.739 (0.009)	0.48	0.09	4,4,5
AS33-1		18 27 12.4	04 02 16	13.180 (0.009)	12.477 (0.004)	12.343 (0.008)	0.84	0.13	4,4,5
AS33-2		18 27 15.5	04 03 34	13.724 (0.024)	13.271 (0.023)	13.168 (0.014)	0.56	0.10	4,4,5
AS34-0	SAO048300	19 17 34.5	48 06 02	8.443 (0.019)	8.434 (0.003)	8.436 (0.019)	0.01	-0.00	3,3,3
AS35-0	SAO070237	20 35 11.2	36 08 49	8.625 (0.009)	8.544 (0.011)	8.524 (0.006)	0.10	0.02	3,4,4
AS36-0	FS29	21 52 25.3	02 23 33	13.168 (0.013)	13.242 (0.007)	13.301 (0.007)	-0.13	-0.06	4,4,4
AS36-1		21 52 26.2	02 24 41	13.538 (0.028)	13.049 (0.012)	12.960 (0.014)	0.58	0.09	3,4,4
AS36-2		21 52 22.4	02 24 32	14.246 (0.014)	13.847 (0.014)	13.737 (0.008)	0.51	0.11	4,4,4
AS36-3		21 52 21.4	02 23 14	14.165 (0.004)	13.607 (0.009)	13.333 (0.022)	0.83	0.27	4,3,4
AS36-4		21 52 25.4	02 23 35	15.312 (0.008)	14.769 (0.006)	14.514 (0.022)	0.80	0.26	4,4,4
AS37-0	SAO072320	22 25 20.7	40 09 38	8.669 (0.017)	8.678 (0.009)	8.635 (0.009)	0.03	0.04	5,5,5
AS37-1		22 25 19.8	40 08 06	11.020 (0.026)	10.516 (0.014)	10.399 (0.011)	0.62	0.12	3,3,3
AS38-0	FS30	22 41 44.7	01 12 36	11.932 (0.006)	11.988 (0.009)	12.027 (0.010)	-0.09	-0.04	5,6,4
AS38-1		22 41 46.4	01 11 52	12.994 (0.004)	12.657 (0.012)	12.588 (0.020)	0.41	0.07	4,5,4
AS38-2		22 41 50.2	01 12 43	11.355 (0.023)	11.026 (0.014)	10.991 (0.013)	0.36	0.04	4,5,4
AS39-0	FS31	23 12 21.2	10 47 06	13.808 (0.008)	13.929 (0.002)	14.011 (0.009)	-0.20	-0.08	5,5,4
AS39-1		23 12 20.7	10 46 36	15.033 (0.022)	14.333 (0.004)	14.045 (0.018)	0.99	0.29	4,4,4
AS40-0	NGC7790	23 58 50.2	61 10 02	11.051 (0.013)	10.408 (0.013)	10.240 (0.013)	0.81	0.17	7,8,8
AS40-1		23 58 43.2	61 10 26	11.900 (0.012)	11.097 (0.011)	10.861 (0.008)	1.04	0.24	7,8,7
AS40-2		23 58 59.7	61 10 26	11.477 (0.018)	10.569 (0.014)	10.314 (0.018)	1.16	0.26	4,4,4
AS40-3		23 58 57.5	61 09 46	10.578 (0.015)	9.966 (0.011)	9.785 (0.008)	0.79	0.18	6,6,6
AS40-4		23 58 53.6	61 11 02	10.356 (0.015)	9.695 (0.008)	9.516 (0.007)	0.84	0.18	7,7,7
AS40-5	23 58 43.2	61 09 42	9.488 (0.013)	9.418 (0.007)	9.405 (0.008)	0.08	0.01	6,6,8	

^aThe three numbers refer to the number of nights in each band, J , H , and K , respectively. The number of nights may differ between bands because of lack of measurements, and may differ between stars of a given field because of bad pixels or positioning of the field on the detector.

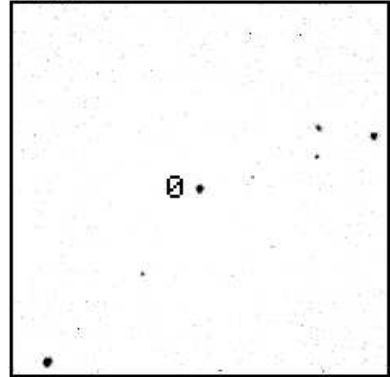
AS01



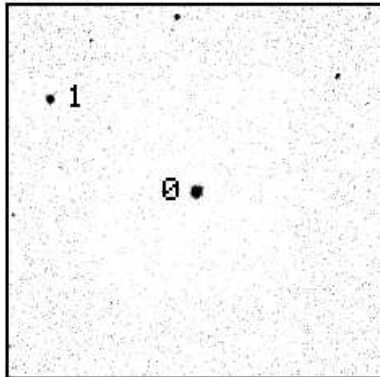
AS02



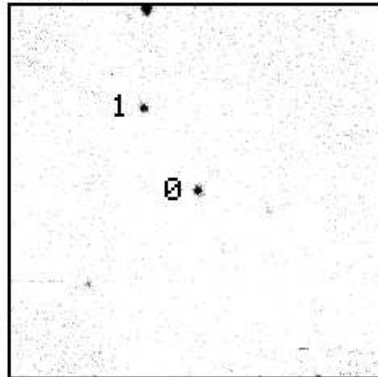
AS03



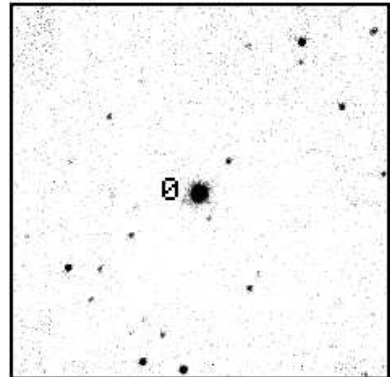
AS04



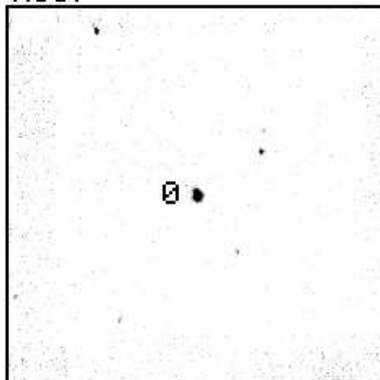
AS05



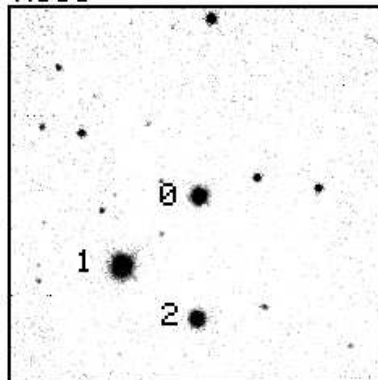
AS06



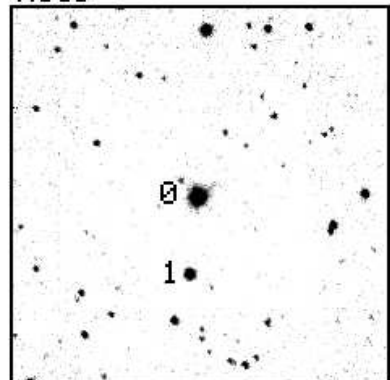
AS07



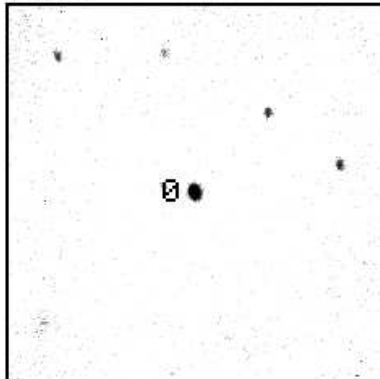
AS08



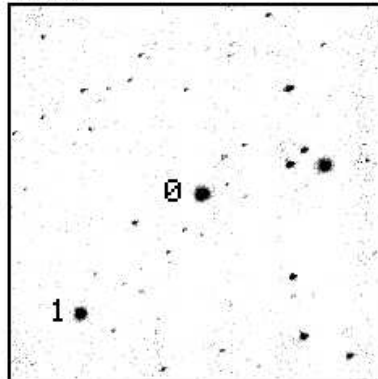
AS09



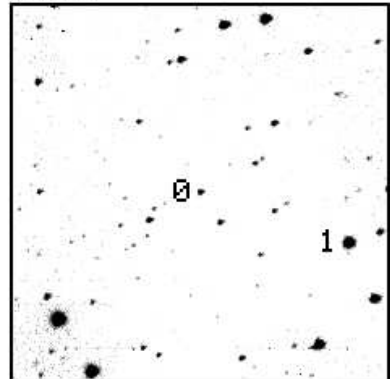
AS10



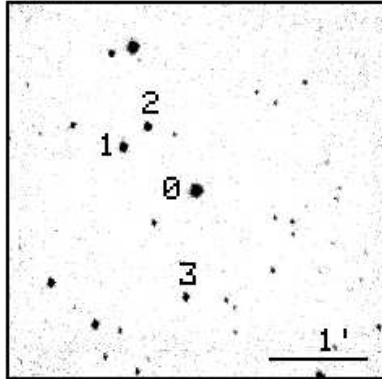
AS11



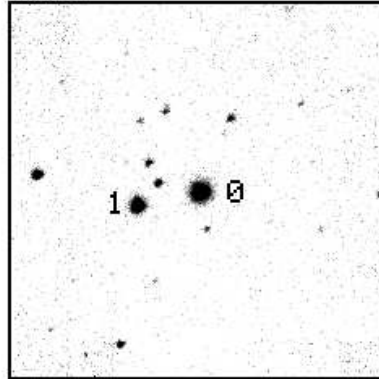
AS12



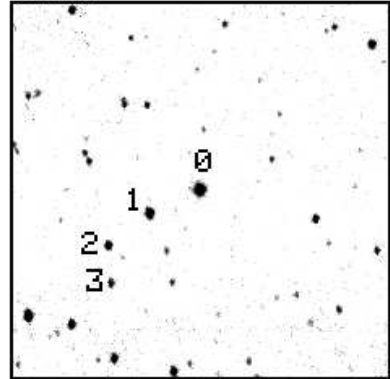
AS13



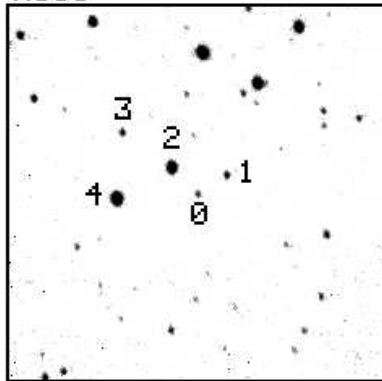
AS14



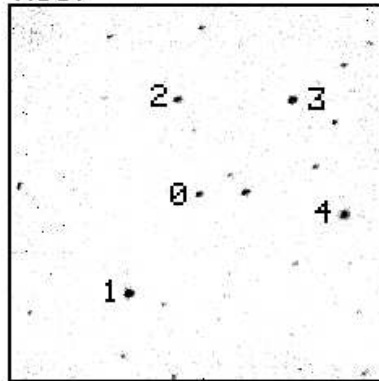
AS15



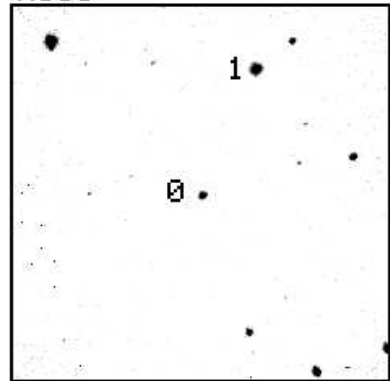
AS16



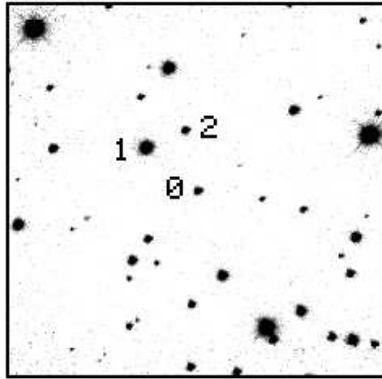
AS17



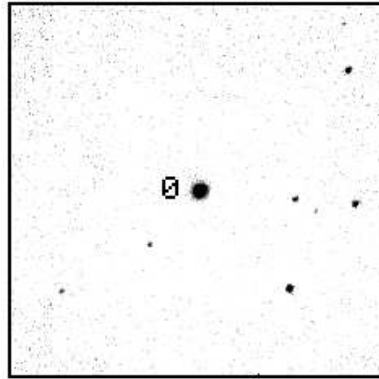
AS18



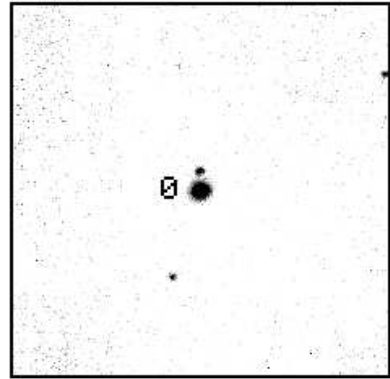
AS19



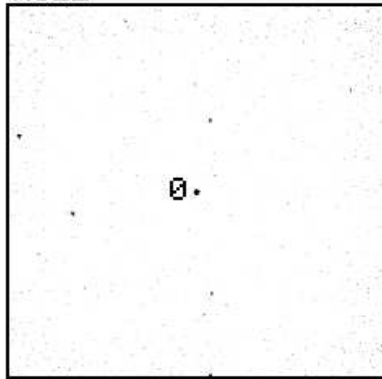
AS20



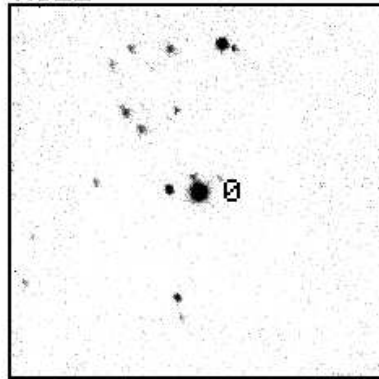
AS21



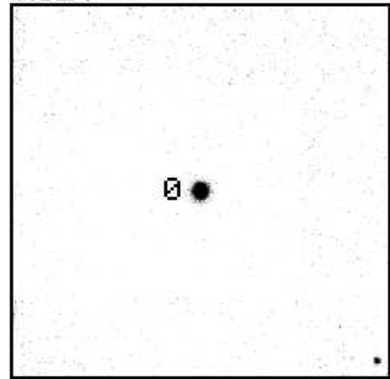
AS22



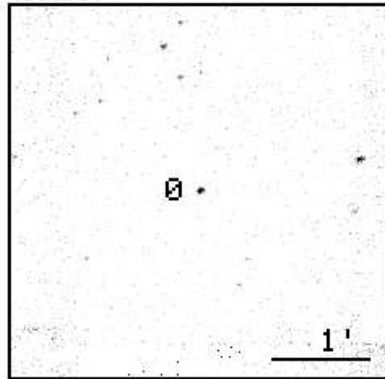
AS23



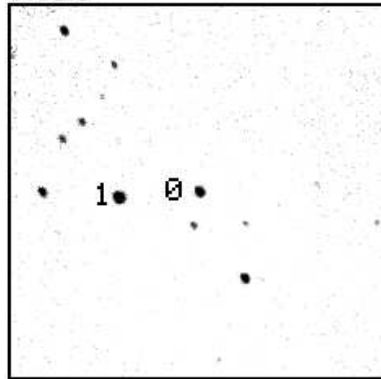
AS24



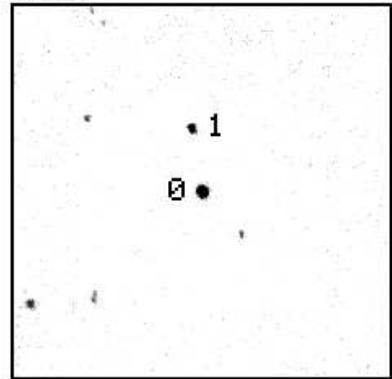
AS25



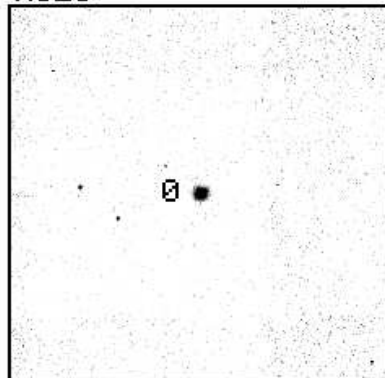
AS26



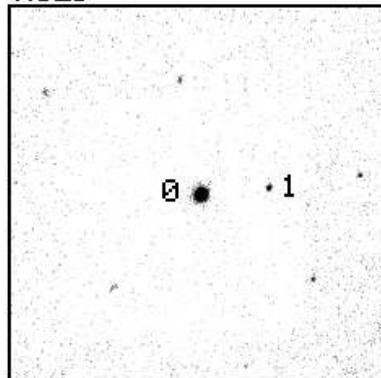
AS27



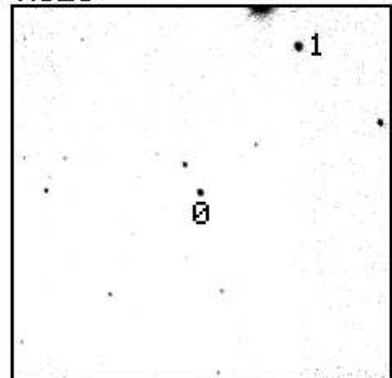
AS28



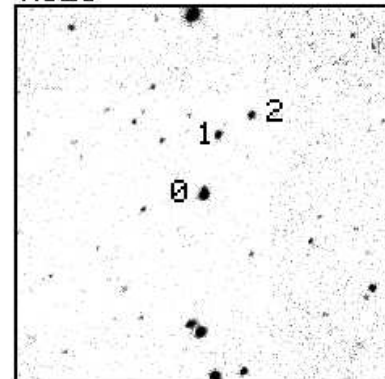
AS29



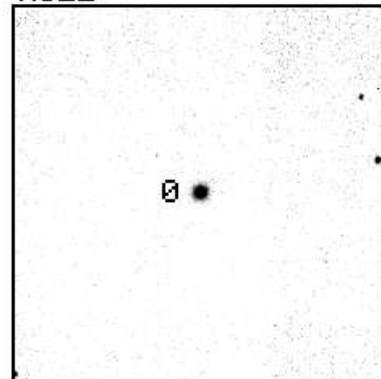
AS30



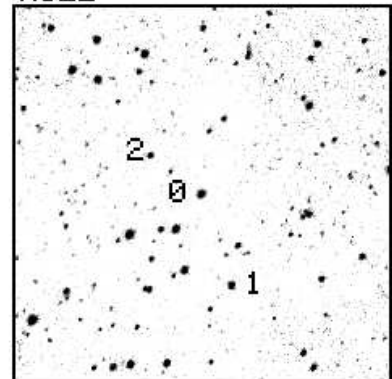
AS31



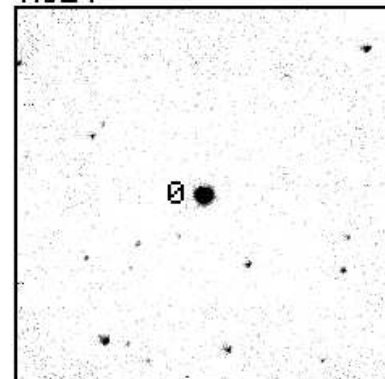
AS32



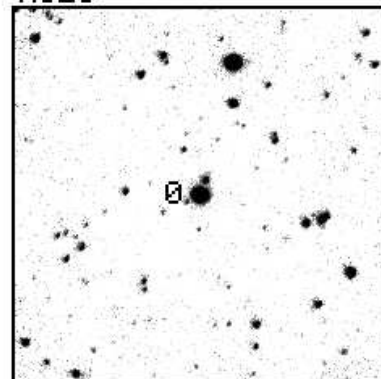
AS33



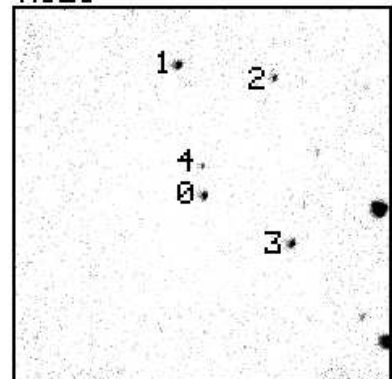
AS34



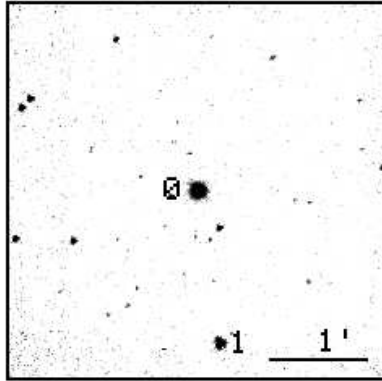
AS35



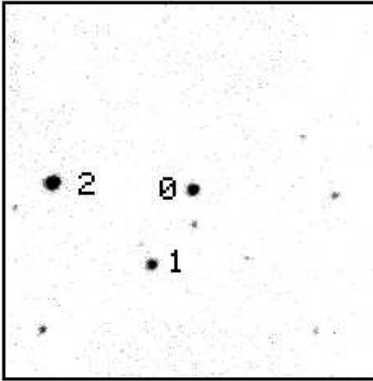
AS36



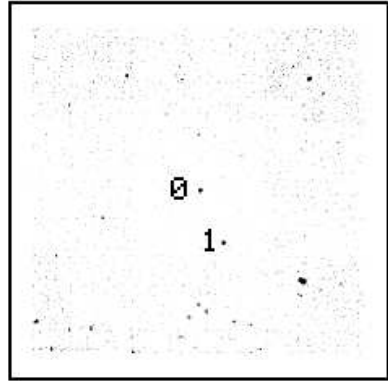
AS37



AS38



AS39



AS40

